npg

Fluorescent microangiography (FMA): an improved tool to visualize the pulmonary microvasculature

Andre E Dutly[1,2,*], Lakshmi Kugathasan[3], Judy E Trogadis[3], Shaf H Keshavjee[2], Duncan J Stewart[3] and David W Courtman[3]

[1]Division of General Thoracic Surgery, University Hospital of Berne, Berne, Switzerland; [2]Thoracic Surgery Research Laboratory, Toronto General Hospital Research Institute, Toronto, ON, Canada and [3]Departments of Surgery and Medicine, Terrence Donnelly Research Laboratories for Cardiovascular Research, St Michael's Hospital, University of Toronto, Toronto, ON, Canada

Visualization of the complex lung microvasculature and resolution of its three-dimensional architecture remains a difficult experimental challenge. We present a novel fluorescent microscopy technique to visualize both the normal and diseased pulmonary microvasculature. Physiologically relevant pulmonary perfusion conditions were applied using a low-viscosity perfusate infused under continuous airway ventilation. Intensely fluorescent polystyrene microspheres, confined to the vascular space, were imaged through confocal optical sectioning of 200 μm-thick lung sections. We applied this technique to rat lungs and the markedly enhanced depth of field in projected images allowed us to follow vascular branching patterns in both normal lungs and lungs from animals with experimentally induced pulmonary arterial hypertension. In addition, this method allowed complementary immunostaining and identification of cellular components surrounding the blood vessels. Fluorescent microangiography is a widely applicable and quantitative tool for the study of vascular changes in animal models of pulmonary disease.
Laboratory Investigation (2006) 86, 409–416. doi:10.1038/labinvest.3700399; published online 20 February 2006

Keywords: confocal microscopy; microvasculature; pulmonary hypertension

The circulatory bed of the lung is uniquely designed to accommodate the entire cardiac output and thus, remodeling of the microvasculature can play a dominant role in the progression of many pulmonary pathologies. For example, pulmonary hypertension (PH) is characterized by a marked increase in vascular resistance, likely resulting from a loss of pulmonary microvessels and/or from excessive smooth muscle hyperplasia in arterioles that normally display only incomplete muscularization.[1] Therefore, obtaining accurate three-dimensional (3D) morphological information on arteriolar and capillary structure along with spatial colocalization of biological mediators will provide fundamental mechanistic insights into the pathogenesis of many pulmonary diseases.[2]

Animal models have been instrumental in the study of pulmonary diseases and numerous rodent models have been established. First generation models have involved toxin-induced pulmonary injuries,[3,4] whereas second and third generation models have been developed with transgenic techniques in combination with environmental or other biological stimuli.[5,6] Such models are powerful tools, yet require specialized techniques in order to efficiently characterize the temporal and spatial patterns of pulmonary pathogenesis. Owing to the technical complexity of current techniques, in-depth characterization of pulmonary microvasculature remodeling has not been performed in these rodent models. Consequently, in order for these models to reach their full potential, newer, readily available techniques need to be developed.

In this study, we present a novel and reproducible method to evaluate the morphometry of the pulmonary circulation and colocalize relevant pathological changes in the surrounding tissue, on a microscopic

410

level. This angiographic technique uses a mixture of low-temperature melting point agarose and fluorescent polystyrene microspheres to produce a low-viscosity infusate targeting the vascular lumens of both the pulmonary and bronchial circulations, independently. Optical sectioning of lung tissue with confocal microscopy yielded accurate 3D vascular geometries and projected images with enhanced depth of field and by applying whole mount histochemical and immunohistochemical techniques we were able to spatially colocalize relevant biological structures with areas of microvascular remodeling.

Materials and methods

Animal Models

All animal experimental procedures were performed in accordance with the Canadian Council on Animal Care guidelines. Fisher-344 rats weighing between 200 and 300 g were used (Charles River Co, St Constant, Quebec, Canada). In the model of monocrotaline (MCT)-induced PH, 75 mg/kg of MCT was injected intraperitoneally and fluorescent microangiograms performed after 3 weeks, the time at which severe PH develops. In the modified orthotopic model of bronchiolitis obliterans (BO), the donor trachea was implanted into the recipient's lung parenchyma, as previously described and angiograms were performed 3 weeks after implantation.

Preparation of Agarose-Bead Perfusate

Low-temperature melting point agarose (100 mg) (Sigma-Aldrich, St Louis, MA, USA) was first dissolved in 9 ml of distilled H_2O at 80°C with constant mixing, followed by the addition of 1 ml of fluorescent polystyrene microspheres (aqueous suspension of 2% solids) (FluoSpheres® Invitrogen, Burlington, ON) into the agarose solution. Yellow–green (505 nm excitation/515 nm emission) or orange (540 nm/560 nm) microspheres ranging in diameters from 0.2 to 10 μm were used in individual experiments as described. The agarose-bead perfusate was loaded into 3 ml syringes and placed in a 45°C water-bath for immediate use or stored at 4°C for later use.

Fluorescent Microangiography

The rats were anesthetized in an isoflurane chamber, and a tracheostomy was performed with a 14-gauge intravenous canula. Animals were continuously ventilated using a volume-controlled ventilator (Model 683; Harvard Rodent Ventilator, South Natick, MA, USA) with a fraction of inspired oxygen (FiO_2) of 1.0, an isoflurane concentration of 1–3%, and a tidal volume of 10 ml/kg at 80 breaths/min. A median sternolaparotomy was then performed, and

500 USP units of heparin (Hepalean®, Organon Teknika, Toronto, Canada) were injected directly into the right atrium. To perfuse the bronchial circulation, the abdominal aorta was transected, and the aortic root canulated and flushed with 20 ml of prewarmed normal saline at a pressure of 40 mmHg. The abdominal aorta was then clamped and 4 ml of the prewarmed agarose-bead mixture containing 0.5 μm-diameter orange polystyrene microspheres was injected into the aortic root at a pressure of 80 mmHg. To perfuse the pulmonary circulation, the right ventricle was canulated *in situ* with a 21-gauge catheter (Terumo Medical Corporation, Elkton, MD, USA) with the tip placed directly into the common pulmonary artery. The inferior vena cava and left atrial appendage were then transected, the aortic root clamped, and the lungs flushed with 20 ml of prewarmed normal saline at a pressure of 25 mmHg. Three ml of the prewarmed agarose-bead mixture containing 0.2 μm-diameter yellow–green polystyrene microspheres was injected at a pressure of 40 mmHg. For prewarmed solutions, filled syringes were maintained in a 45°C water bath until use. Temperature losses during syringe attachment to the catheter and subsequent injection resulted in a maximum lung temperature of between 37 and 39°C. Upon complete injection of the perfusate, ventilation was stopped and the animal's chest was covered with crushed ice in order to enhance gelling of the perfusate. The heart–lung block was then removed and 6 ml of cold 4% paraformaldehyde (PFA) was injected intratracheally. Following 24 h of fixation, the specimen was rinsed and stored in 70% ethanol.

Immunofluorescence and Confocal Microscopy

Cross-sections (200 μm-thick) of the left lobe of all lungs were cut using a vibrating-blade microtome (VT100SR, Leica, Nussloch, Germany). Cutting speed was set at less then 0.025 mm/s and vibration frequency was set at 100 Hz. Nuclear counterstaining was performed by incubating sections in the dark for 20 min with either 1 μg/ml propidium iodide (PI) or 1 μM To-Pro-3 (Invitrogen, Burlington, ON) with gentle agitation. The sections were then rinsed well in phosphate buffered saline (PBS) and mounted on glass slides with *Mowiol*, a polyvinyl alcohol mounting medium (Mowiol, Calbiochem, San Diego, CA, USA) containing 2.5% (wt/vol) DABCO antifading agent (Sigma). For smooth muscle alpha-actin (SMA) and laminin staining, sections were first treated with blocking solution (5% bovine serum albumin (BSA) with 0.2% Triton-X in PBS) for 1 h at room temperature. The solution was then replaced with a 1:100 dilution of SMA monoclonal antibody (Neomarkers, Fremont, CA, USA) or 1:100 of laminin Ab-1 rabbit polyclonal antibody (Medicorp, Montreal, Quebec, Canada) both diluted in blocking solution and incubated on a rocker over-

night, at 4°C. Sections were then rinsed, incubated with a Cy3 conjugated goat antimouse IgG or donkey anti-rabbit IgG (Jackson Immunological) as appropriate and mounted in Mowiol mounting medium with DABCO antifading agent.

Optical sectioning was performed on a Bio-Rad Radiance^R confocal microscope (Carl Zeiss Ltd, Toronto, Canada) by collecting a z-series (5–10 μm steps) through the 200 μm-thick lung sections. Data were displayed either as a projected image or an animated sequence, or as a single section, for further analysis. Yellow–green fluorescent microspheres were viewed with an argon laser (488 nm) at an emission of 515 nm (30 nm band pass); orange microspheres, PI nuclear staining, and SMA were detected with a green HeNe laser (543 nm) at greater then 600 nm emission; and To-Pro3 nuclear stain visualized with a red diode laser (633 nm) at emissions above 640 nm.

Image Analysis

To quantitate microvessel density, pixel intensity values were analyzed in single optical sections (16 μm from the surface), using Image J (NIH, Bethesda, MD, http://rsb.info.nih.gov/ij/). Images were uniformly thresholded setting a lower limit and maximum upper limit, and measurements counted the number of thresholded pixels. Large distributing vessels were excluded from analysis. Digital confocal images were further analyzed using Adobe Photoshop with Image Processing Toolkit (Reindeer Graphics, Inc., Asheville, NC, USA) plugins.[8] To compare the density of vessels in normal and MCT-treated animals, the colored images were separated (Channels/Split channels) and further image processing was carried out only on 8-bit grayscale images of fluorescently labeled vessels. Following the application of a blurring filter to reduce noise (Filter/Blur/Gaussian $r = 1$), the images were thresholded to choose the pixel intensity range most representative of filled vessels—determined as 128—and was used for all subsequent images to include or exclude points (Image/Adjust/Threshold—128). The fluorescent images were inverted for further analysis with IPTK plugin filters (Image/Adjust/Invert) and an erode filter applied to eliminate noise and single pixels (Filter/IP*Morphology/Erode). Subsequently, a skeletonized frame representation of the arterial branching pattern was obtained (Filter/IP*Morphology/Skeletonize), with each branch depicted as a single pixel width black line. The final measurement (Filter/IP*Measure/Total length) provided a quantitative assessment of vessel length and density by measuring the total vessel length, the number of branching nodes and the number of ends. The number of vessels was then calculated by taking the sum of the ends and nodes and dividing it by two: total vessel number = (ends + nodes)/2.

Results

In an initial series of experiments, the optimal agarose concentration, bead size, concentration, perfusion pressure, and total amount of perfusate were determined. We found that using agarose concentrations of 1% produced excellent perfusion and sectioning characteristics while maintaining a fluid viscosity approximating that of blood, while higher agarose concentrations resulted in decreased perfusion due to the high viscosity. Polystyrene microspheres with diameters larger than 5 μm plugged the smaller vessels and resulted in only partial, heterogeneous filling of the vasculature. Dispersion of the lipophylic dye within the hydrophobic environment of the microsphere limited oxygen diffusion and consequently enhanced fluorescent intensity. This allowed us to use a low concentration (0.2% solids) of beads in the perfusate while maintaining optimal imaging characteristics and low viscosity. We found that homogenous perfusion was best achieved when the mixture of agarose–polystyrene microspheres was injected at a pressure of 40 mmHg with continuous ventilation. Ventilation throughout the entire procedure was critical to reduce vascular resistance and produce a perfusion reflecting that of the physiological state. We also found that optimal tissue texture for thick sectioning was only produced following a 12–24 h fixation with 4% phosphate buffered PFA.

To distinguish between the pulmonary and bronchial circulations simultaneously, we injected yellow–green polystyrene microspheres into the pulmonary circulation and orange polystyrene microspheres into the aortic root. To obtain an overall image of pulmonary morphology, a composite confocal image of an entire transverse lung section was created by collecting confocal z-series (spanning 100 μm depth) of 16 individual, overlapping fields of view. Projections were created from each z-series and Adobe Photoshop (Adobe Inc., Mountainview, CA, USA) was used to produce a montage from the individual projections (Figure 1). Figure 1 illustrates a
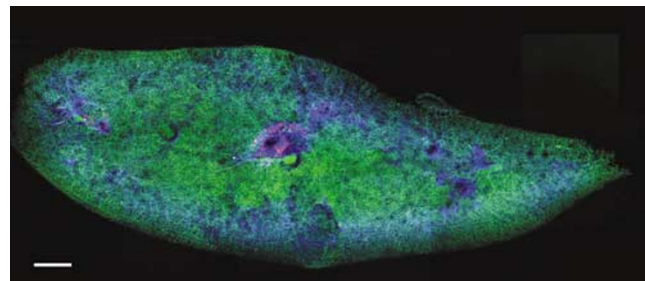
Figure 1 Composite transverse section from the left lobe of a rat lung. This image was created from projections of individual z-series of overlapping adjacent areas of a 200 μm-thick section. Yellow–green fluorescent micropheres in agarose fill the pulmonary vasculature (green) and orange microspheres fill the bronchial circulation (red). The section was counter-stained with the nuclear dye To-Pro-3 (blue). Scale bar = 200 μm.
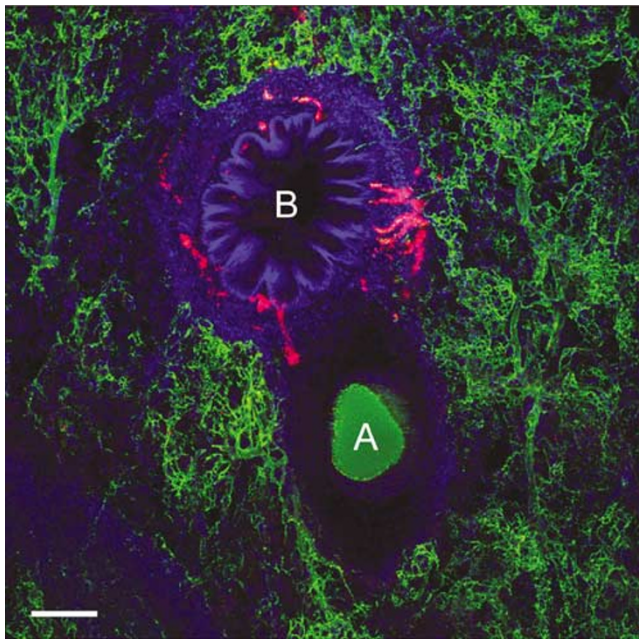
Figure 2 Pulmonary and bronchial circulations. This high power projection of a large bronchus (B), adjacent pulmonary artery (A), and surrounding parenchyma displays yellow-green fluorescent microspheres filling the pulmonary circulation (green) and orange microspheres filling the bronchial circulation (red). Scale bar = 50 μm.

complete perfusion yet displays a heterogeneous vascular density, higher in the central regions, characteristic of normal lung architecture. In Figure 2, a high-power field of the central bronchial region indicates the perfusion of the bronchial vascular bed independently from the pulmonary circulation, consistent with the anatomical separation of these two arterial systems.

Normal rats and those with established PH (3 weeks post-MCT) were perfused through the pulmonary artery with agarose containing yellow–green microspheres and 200 μm-thick sections were counterstained with PI (Figure 3). Hypertensive rats displayed decreased capillary filling and arteriolar wall thickening. Computerized digital analysis was used to quantitate the pulmonary vascular morphometry.[8] Using Photoshop, images were thresholded for a representative fluorescent intensity range, and the filters in the Image Processing Toolkit plugins were further used to display a skeletonized frame of the vascular architecture (see Materials and methods for details). A final measurement provided a quantitative assessment of vessel density by measuring total length and number of branches. In our example of a normal vessel (Figure 3b), calculation of the results of the skeletonization process produced a total count of 1246 ends and 493 nodes, and a total of 870 vessels. Similar calculations in the vessels of an MCT-treated animal (Figure 3e) resulted in 208 ends, 42 nodes, and a total vessel number of 175. Pixel counts of vascular structure

from single optical sections resulted in 54.5 ± 7.5 for normal and 17.6 ± 2.3 for MCT-treated rats (thousands of pixels per section, $n = 10$ rats per group, $P < 0.05$). Therefore, both analytical techniques demonstrated a marked decrease in vascularity for MCT-treated animals.

Three-dimensional reconstructions of the normal and hypertensive pulmonary vasculature were generated from image stacks of 75 sections with a 1 μm step size using the Volume J plugin of ImageJ (NIH, Bethesda, MD, USA). Representative 2D perspective views as shown in Figure 4 highlight the marked loss of vasculature in MCT-treated animals. Movies of image rotation have been provided as a Web Supplement online at http://www.nature.com/labinvest.

Arteriolar muscularization was examined by immunostaining with a smooth muscle-specific alpha-actin antibody (Figure 5a). This staining showed the extent of continuous smooth muscle cell coverage within the arterial tree, with full muscularization extending down to the branching point immediately before the precapillary arterioles. Distal to this point, smooth muscle cell coverage was no longer continuous, although some smooth muscle cells were evident even at the level of capillary branching.

The microvascular structures of the alveoli were clearly distinguished by fluorescent angiography combined with basement membrane labeling with a laminin-specific antibody (Figure 5b). Air spaces are easily identified and perfusion through the alveolar septi can be readily observed. A high degree of colocalization of flow with basement membrane structures is evident.

In order to investigate the angiogenic capacity of the pulmonary circulation, a model of fibrous airway obliteration (BO),[7] in which a trachea was implanted into the lung parenchyma, was utilized. Yellow–green microspheres were injected either into the pulmonary artery or aortic root. Confocal analysis demonstrated robust vascularization of the tracheal graft and, contrary to the current understanding of angiogenesis in the lung, the implanted tracheas were found to be perfused principally from the pulmonary and not from the systemic circulation (Figure 6).

Discussion

The most common technique employed to study the pulmonary vasculature involves histological staining of thin sections. However, the tortuous nature of pulmonary vessels makes it impossible to define and track individual blood vessels in a single thin section. Although reconstruction of 3D structures can be achieved from serial sectioning, this method is tedious, prone to errors, and thus seldom employed. Barium sulfate–gelatin infusions have also been traditionally used for low-resolution
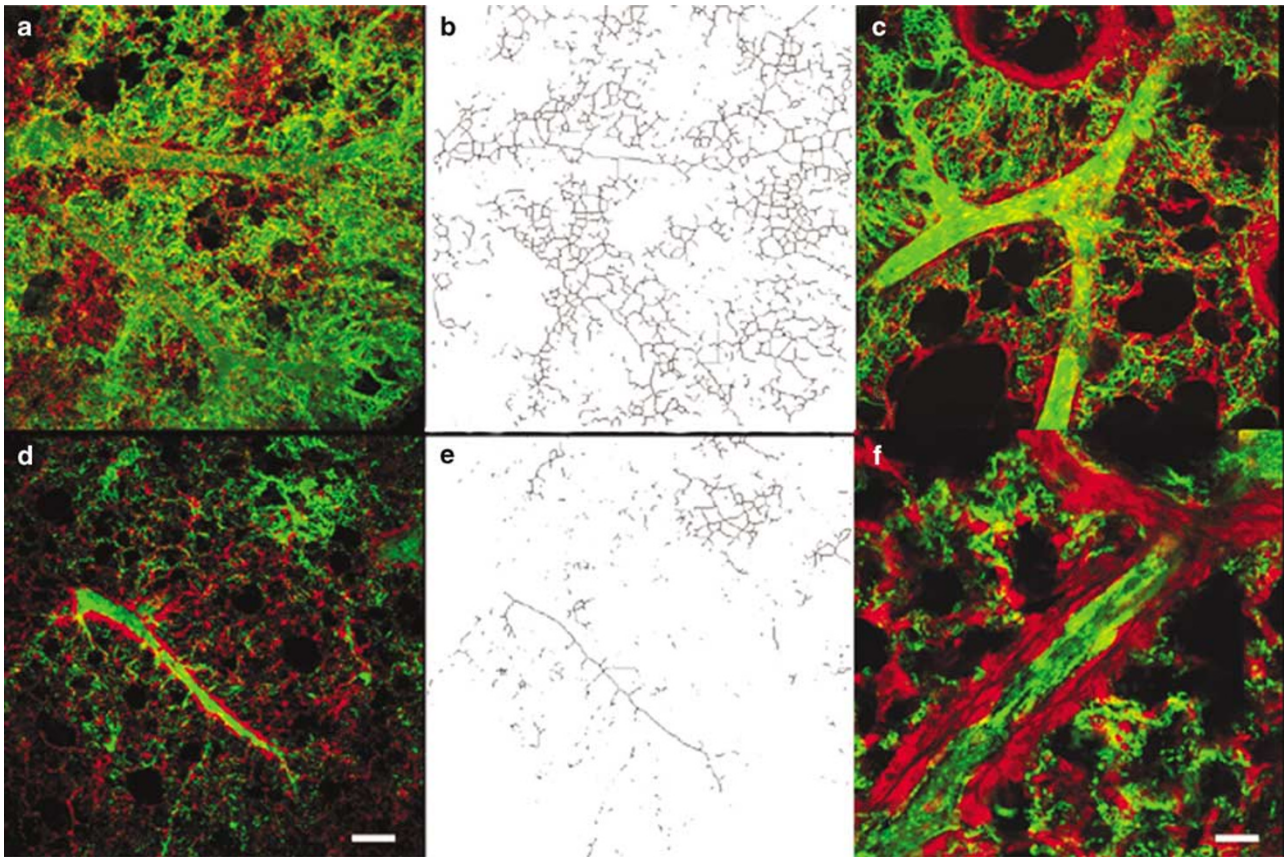
Figure 3 Analysis of pulmonary vessel density in normal and MCT treated rats. The pulmonary vasculature was infused with yellow-green microspheres (green) and thick sections counterstained with propidium iodide (red). Vessels from normal rats (**a–c**) showed extensive branching, while MCT-treated specimens (**d–f**) showed a reduction in both vessel number and branching. A skeletonizing filter which allows the conversion of branches to single pixel width lines, defines total length and counts branching nodes, clearly demonstrating the decrease in complexity of the pulmonary vasculature. Higher magnification images highlight vessel wall thickening, represented by increased propidium iodide staining in MCT-treated (**f**) animals compared to normal (**c**). Scale bar in (**a**) and (**d**) = 100 μm; (**c**) and (**f**) = 50 μm.

arteriograms and to identify pulmonary arteries following histological sectioning.[9–14] However, in addition to the drawbacks of histological sectioning, the high viscosity of the barium mixture (as much as 100–300 centipoise) necessitates the use of an artificially high perfusion pressure resulting in distension of the proximal vasculature. In contrast, our technique uses an agarose mixture with a viscosity similar to that reported for the relative blood viscosity in the microvasculature (less then 5 centipoise at 37°C);[15] and the optimal perfusion pressure for this mixture was found to be at 40 mmHg. The lung, unlike other tissues, regulates perfusion through the recruitment of vascular beds in a ventilation-dependent manner. We believe the use of our optimum perfusion pressure with constant ventilation produces a physiologically relevant filling of the lung parenchyma.

Corrosion casting of the vasculature with polymers such as methyl methacrylate and subsequent tissue removal with corrosive alkalis produces accurate 3D casts of the vasculature; however, because all surrounding tissue structure is de-stroyed, it becomes difficult to identify areas of active vascular remodeling.[16,17] In our technique, tissue is preserved and vascular casting can be combined with whole mount histochemical and immunohistochemical techniques to spatially localize cellular processes involved in vascular remodeling. In addition, this fluorescent technique is easily performed and allows for segmental biochemical analysis of pulmonary tissue from the same animal.

The lung is unique in that perfusion arises from both the pulmonary and systemic (bronchial) circulations. Pulmonary disease is often associated with remodeling of the vasculature and this may involve one or both of these circulatory systems. Our technique is ideally suited to differentiate remodeling processes (such as angiogenesis, capillary loss, or arteriolar thickening) in either vascular system. Prevalent diseases such as chronic obstructive pulmonary disease (COPD), emphysema, and asthma all display differential involvement of the bronchial and pulmonary circulations.[18,19] Thus, a complete characterization of differential vascular

414
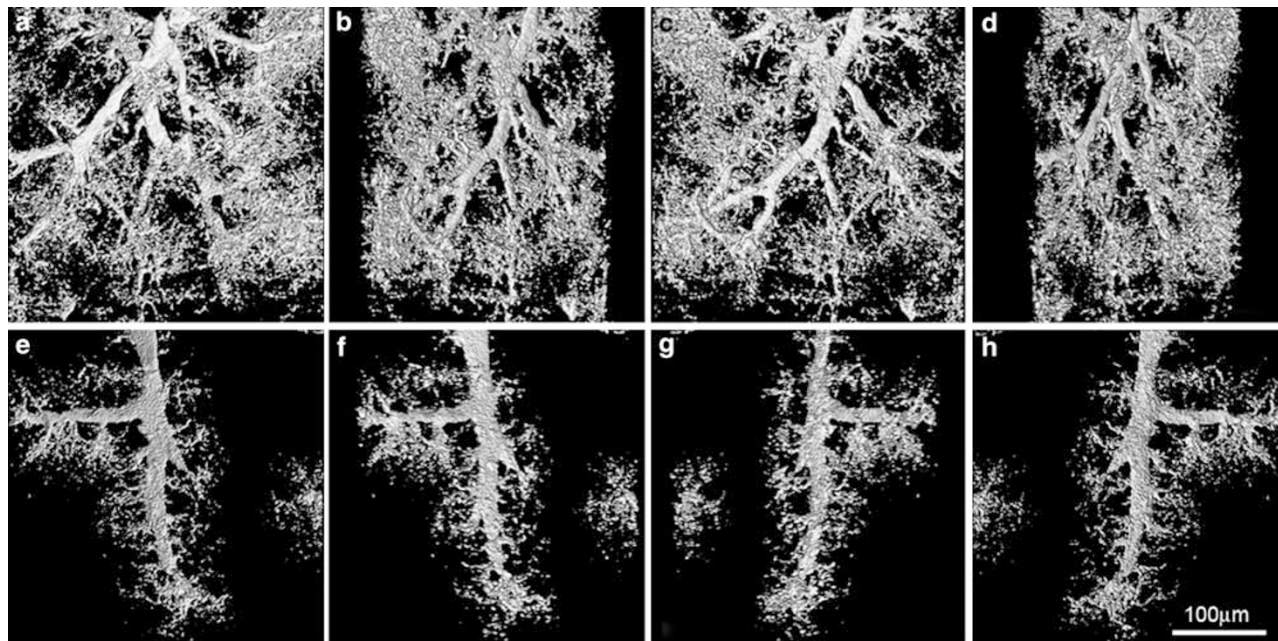
Figure 4 Three-dimensional reconstruction. Representative two-dimensional views from 3D reconstruction of the normal (**a–d**) and MCT treated (**e–h**) rat pulmonary vasculature are displayed. 75 optical sections (1 μm step size) were used to construct the image views, note the marked loss of vasculature in the pulmonary hypertensive MCT treated lung. Additional 3D animations can be viewed online as Supplements at http://www.nature.com/labinvest.
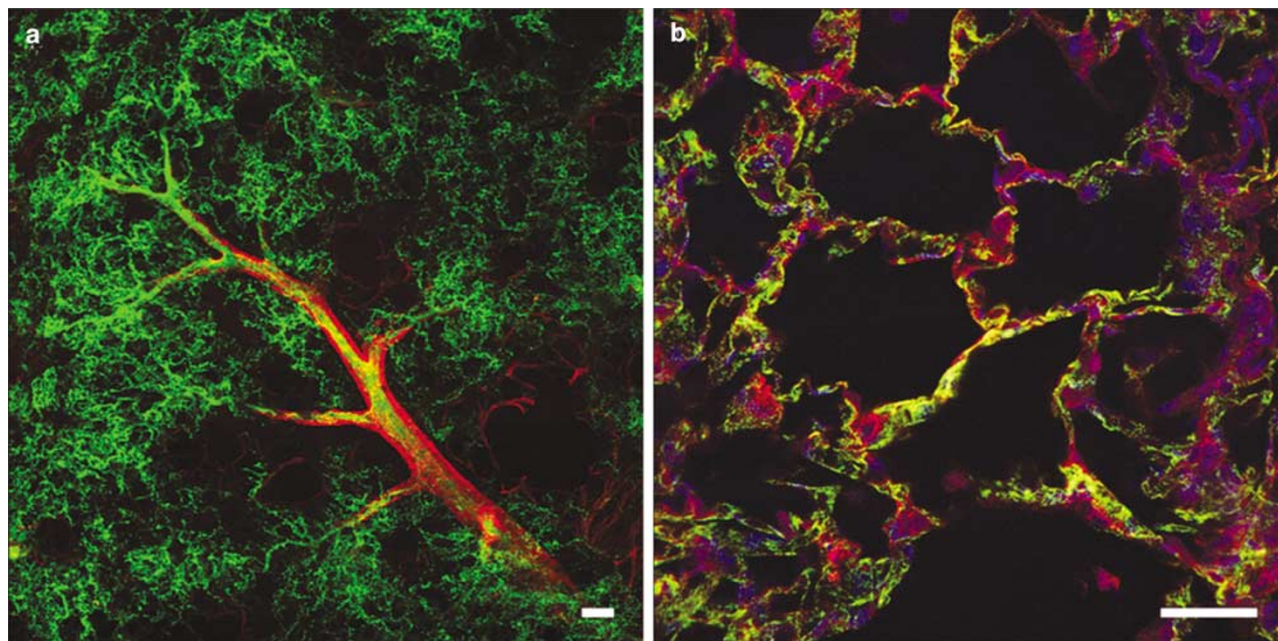

Figure 5 Combined Angiography and Immunostaining. Microsphere perfusion (green) was combined with thick section immunostaining for either smooth muscle alpha-actin or laminin (both red). Smooth muscle staining (**a**) revealed the extent of muscularization in the normal rat lung. Laminin staining (**b**) displayed the perfusion profile in the alveolar septi (blue is nuclear counterstaining). Both images are projections of a confocal z-series taken through a 200 μm section. Scale bars $= 100\,\mu$m.

remodeling will be critical to the development of new animal models and treatments.

The fluorescent angiography described here is amenable to quantitative analysis. The technique uses highly fluorescent beads, which are solely confined to the vascular space eliminating fluorescent dye diffusion into the surrounding tissue and allowing for accurate measurement of lumen diameter. We have tested several different sizes of microspheres and found that both 0.2 and 0.5 μm
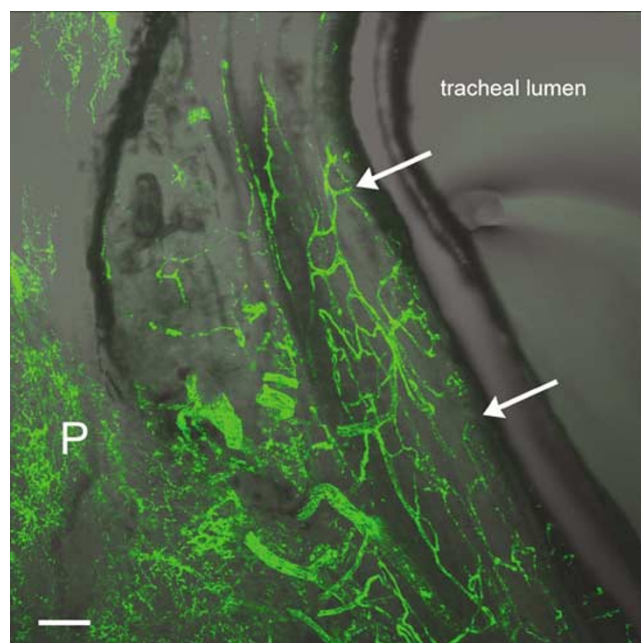
Figure 6 Post Transplant Vascular Remodeling: A tracheal transplant model of obliterative airway disease was used to examine angiogenic responses in the rat lung. A composite image was generated by merging a brightfield and a fluorescent image from a thick section. Perfusion through the pulmonary artery produced filling of vessels within the wall of the transplanted trachea (green fluorescence). These vessels extended from the lung parenchyma (P) into the subepithelial layers of the transplanted trachea (arrows). Scale bar = 100 μm.

spheres work equally well. We routinely use the 0.2 μm particles to ensure that they remain within the vascular space, and are the smallest capable of doing so allowing for complete dispersion throughout even the smallest capillaries. Previous studies have investigated trans-capillary permeability to different sizes of particles (carbon, ferritin, hemoglobin, and myoglobin), demonstrating that carbon tracers of 25–50 nm diameter show no extravasation even in the most fenestrated capillaries or in capillaries challenged by histamine yet smaller ferritin paricles (11 nm diameter) do extravasate.[20] Thus, our 200 nm fluorescent microspheres represent the best balance between perfusion and intravascular retention.

By using confocal microscopy we are able to generate projected images which accurately reflect vessel geometry within the 3D space of our thick sections. Stacks of images can be analyzed as projections by use of branching models as we have performed in Figure 3 or if over sampling is a concern, spatially distinct multiple optical sections can be independently analyzed. Several different mathematical models have been employed to quantitatively describe the pulmonary vasculature. One of these, the diameter-defined modification to the Strahler system, assigns a numeric order of increasing numbers starting at vessels with the smallest

diameter and incrementing values as they meet other branches along an ascending artery or vein.[21] Although we have not measured diameters of the vessels in this study we did use an unbiased method of estimating density of vessels of different sizes by use of a skeletonizing algorithm.[8] This image processing technique provided highly significant differences in vessel number in comparing thick sections from normal and MCT-treated animals. A simple analysis of pixel intensity within any single optical section is biased by both vessel number and size, yet may be a better reflection of total vascular volume, and such an analysis on our samples also revealed marked differences between normal and pulmonary hypertensive rats. Taken together, these results suggest that a loss of vessels in addition to vascular constriction occurs in this MCT induced disease process.

The potential for optical artefacts exists with any microscopic technique and these can be significant when analyzing deeper tissue structures. Epifluorescent confocal microscopy is well suited for analysis of thick sections as out of focus signals are almost completely removed, yet attenuation of either the illumination or emission signals may complicate quantitative analysis. In our procedure we have used 'intensely fluorescent fluorospheres' from Molecular Probes. These polystyrene microspheres shield the highly concentrated dye from oxidative reactions leading to a stable and extremely bright fluorescent intensity. This intense fluorescence allows us to probe deep into the tissue, moreover, *in vitro* experiments with fluorosphere filled glass capillaries demonstrate that this penetration is as much as 10 times greater then that of a standard fluorophore (FITC). Thus, caution must be used when interpreting combined immunofluorescence and microangiography as emissions from standard fluorophores in deeper structures are likely to be attenuated. The highly fluorescent microspheres may also induce the phenomenon of self shadowing[22] in effect attenuating the excitation signal and the resulting fluorescence. Such shadowing may appear as central darkening in larger vessels as in some areas of Figure 2. However, it has been our experience that careful optimization of image collection parameters can markedly limit these potential artefacts.

In summary, we present a new technique of fluorescent-agarose-based angiography to visualize and quantitatively analyze the pulmonary microvasculature. In comparison to currently available tools, this methodology is readily employable, accurately reflects physiological perfusion, and can easily be extended to include additional tissue analyses. Finally, this technique provides an available and useful tool for understanding the mechanisms underlying pulmonary diseases and with adaptations, can also be applied more widely to include different organ systems in other animal models.

416

References

1 Pietra GG, Capron F, Stewart S, *et al.* Pathologic assessment of vasculopathies in pulmonary hypertension. J Am Coll Cardiol 2004;43:25S–32S.

2 Finlay M, Barer GR, Suggett AJ. Quantitative changes in the rat pulmonary vasculature in chronic hypoxia—relation to haemodynamic changes. Q J Exp Physiol 1986;71:151–163.

3 Campbell AI, Kuliszewski MA, Stewart DJ. Cell-based gene transfer to the pulmonary vasculature: Endothelial nitric oxide synthase overexpression inhibits monocrotaline-induced pulmonary hypertension. Am J Respir Cell Mol Biol 1999;21:567–575.

4 Kononov S, Brewer K, Sakai H, *et al.* Roles of mechanical forces and collagen failure in the development of elastase-induced emphysema. Am J Respir Crit Care Med 2001;164:1920–1926.

5 West J, Fagan K, Steudel W, *et al.* Pulmonary hypertension in transgenic mice expressing a dominant-negative BMPRII gene in smooth muscle. Circ Res 2004;94:1109–1114.

6 Le Cras TD, Hardie WD, Deutsch GH, *et al.* Transient induction of TGF-alpha disrupts lung morphogenesis, causing pulmonary disease in adulthood. Am J Physiol Lung Cell Mol Physiol 2004;287:L718–L729.

7 Dutly AE, Andrade CF, Verkaik R, *et al.* A novel model for post-transplant obliterative airway disease reveals angiogenesis from the pulmonary circulation. Am J Transplant 2005;5:248–254.

8 Wild R, Ramakrishnan S, Sedgewick J, *et al.* Quantitative assessment of angiogenesis and tumor vessel architecture by computer-assisted digital image analysis: effects of VEGF-toxin conjugate on tumor microvessel density. Microvasc Res 2000;59:368–376.

9 Jakkula M, Le Cras TD, Gebb S, *et al.* Inhibition of angiogenesis decreases alveolarization in the developing rat lung. Am J Physiol Lung Cell Mol Physiol 2000;279:L600–L607.

10 Hasegawa I, Kobayashi K, Kohda E, *et al.* Bronchopulmonary arterial anastomosis at the precapillary level in human lung. Visualization using CT angiography compared with microangiography of autopsied lung. Acta Radiol 1999;40:578–584.

11 Kanai M, Kitano Y, von Allmen D, *et al.* Fetal tracheal occlusion in the rat model of nitrofen-induced congenital diaphragmatic hernia: tracheal occlusion reverses the arterial structural abnormality. J Pediatr Surg 2001;36:839–845.

12 Tang JR, Le Cras TD, Morris Jr KG, *et al.* Brief perinatal hypoxia increases severity of pulmonary hypertension after reexposure to hypoxia in infant rats. Am J Physiol Lung Cell Mol Physiol 2000;278:L356–L364.

13 Todd L, Mullen M, Olley PM, *et al.* Pulmonary toxicity of monocrotaline differs at critical periods of lung development. Pediatr Res 1985;19:731–737.

14 Le Cras TD, Kim DH, Gebb S, *et al.* Abnormal lung growth and the development of pulmonary hypertension in the Fawn-Hooded rat. Am J Physiol 1999;277: L709–L718.

15 Fung Y. Biomechanics: Mechanical Properties of Living Tissues. Springer-Verlag: London, 1990.

16 Bennett SH, Eldridge MW, Zaghi D, *et al.* Form and function of fetal and neonatal pulmonary arterial bifurcations. Am J Physiol Heart Circ Physiol 2000; 279:H3047–H3057.

17 Caduff JH, Fischer LC, Burri PH. Scanning electron microscope study of the developing microvasculature in the postnatal rat lung. Anat Rec 1986;216: 154–164.

18 Asai K, Kanazawa H, Otani K, *et al.* Imbalance between vascular endothelial growth factor and endostatin levels in induced sputum from asthmatic subjects. J Allergy Clin Immunol 2002;110:571–575.

19 Kasahara Y, Tuder RM, Cool CD, *et al.* Endothelial cell death and decreased expression of vascular endothelial growth factor and vascular endothelial growth factor receptor 2 in emphysema. Am J Respir Crit Care Med 2001;163:737–744.

20 Milici AJ, Bankston PW. Fetal and neonatal rat intestinal capillaries: permeability to carbon, ferritin, hemoglobin, and myoglobin. Am J Anat 1982;165: 165–186.

21 Huang W, Yen RT, McLaurine M, *et al.* Morphometry of the human pulmonary vasculature. J Appl Physiol 1996;81:2123–2133.

22 Pawley J (ed). Handbook of Biological Confocal Microscopy, 2nd edn. Plenum Press: New York, 1995.